Czerny-Turner imaging spectrometer for broadband spectral simultaneity

Qingsheng Xue (薛庆生)[1,2*], Shurong Wang (王淑荣)[1], and Futian Li (李福田)[1]

[1]*State Key Laboratory of Applied Optics, Changchun Institute of Optics, Fine Mechanics and Physics, Chinese Academy of Sciences, Changchun 130033, China*

[2]*Graduate University of Chinese Academy of Sciences, Beijing 100049, China*

[*]*E-mail: qshxue2006@163.com*

Received December 1, 2008

A modified asymmetrical Czerny-Turner arrangement with a fixed plane grating is proposed to correct aberrations over a broadband spectral range by analyzing the dependence of aberrations for different wavelengths. The principle of design is deduced in detail. We compare the performance of this modified Czerny-Turner imaging spectrometer with that of the existing Czerny-Turner arrangement by using a practical Czerny-Turner imaging spectrometer example. The excellent performance of the modified imaging spectrometer is confirmed by simulation with ZEMAX software.

OCIS codes: 300.6190, 120.0280, 120.6200, 220.1000, 220.4830.

doi: 10.3788/COL20090709.0861.

Czerny-Turner spectrograph has been studied and applied by some authors[1−5] both in its classical form (spherical mirrors and symmetrical design) and different modifications. Several Czerny-Turner spectrographs using focal plane array detectors have flown in space, e.g., the Middle Atmosphere High Resolution Spectrograph Investigation (MAHRSI)[6] and the Shuttle Ozone Limb Sounding Experiment (SOLSE)[7]. MAHRSI utilized a scanned grating with the wavelength ranging from 0.19 to 0.32 μm, for which the grating must be scanned to cover the whole spectral region of the instrument. SOLSE demonstrated the feasibility of using charge-coupled device (CCD) technology to eliminate moving parts in simpler, cheaper, ozone-mapping instruments. SOLSE permitted simultaneous acquisition of a multi-wavelength image from 0.275 to 0.36 μm. It is remarkable that in all existing Czerny-Turner arrangements the grating is placed in the vicinity of the focal plane of the mirrors. For these positions of grating, the aberrations depend on the wavelength and therefore the useful spectral range decreases considerably. However, some optical spectroscopic measurement and remote-sensing applications (e.g., thermospheric/ionospheric studies[8] and limb scattering measurement[9]) require simultaneously obtaining broadband spectral image ($0.35 - 0.75$ μm) with a fixed dispersive element. Thus the existing Czerny-Turner spectrograph cannot fulfill the requirements. Therefore, we study the optical design of the Czerny-Turner spectrometer to correct aberrations substantially over a broadband spectral range with a fixed grating (not a scanning grating). In this letter, a novel arrangement is given by analyzing the dependence of aberrations for different wavelengths. It is confirmed that the modified arrangement found here is better than the existing arrangements.

The spectrometer discussed in this letter is shown in Fig. 1. It consists of two concave mirrors and one plane grating. The object is a slit. The slit is imaged by the system into several images with each one corresponding to a different wavelength. The grating is an aperture stop without aberration correction. That is, the groove size is constant and no cylindrical power is added to the grating. The directions of diffracted light of the grating satisfy the Bragg relation:

$$\sin i + \sin \theta = m\lambda p, \tag{1}$$

where i is the incident angle, θ is the diffraction angle for the diffraction order m, λ is the wavelength, and p is the number of grooves in a unit length.

To study the imaging properties of this system, we will derive the aberration expressions of the full system. The coordinate system for calculation of aberrations is shown in Fig. 2. $A_{\rm o}$ is an object point in the object plane, A is an ideal image point, and A' is a real image point in Gaussian image plane. Aberrations can be expressed by geometrical aberrations or wavefront aberrations. The primary geometrical aberrations can be expressed by[10]

$$\begin{aligned} 2nuTA_y = {} & S_{\rm I} y(y^2 + x^2) + S_{\rm II}\eta(3y^2 + x^2) \\ & + (3S_{\rm III} + S_{\rm IV})\eta^2 y + S_V \eta^3), \end{aligned} \tag{2}$$

$$\begin{aligned} 2nuTA_x = {} & S_{\rm I} x(y^2 + x^2) + S_{\rm II}\eta(2yx) \\ & + (S_{\rm III} + S_{\rm IV})\eta^2 x. \end{aligned} \tag{3}$$

where n is the refractive index; u is the semi-aperture

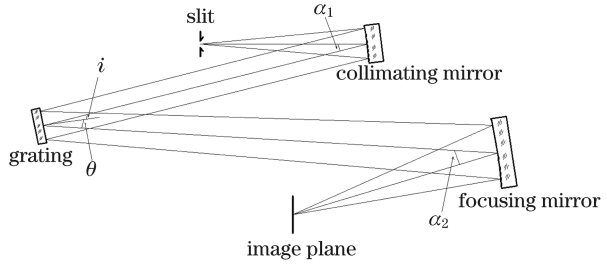

Fig. 1. Two-dimensional schematic of Czerny-Turner imaging spectrometer.

angle of ray; $S_{\rm I}$, $S_{\rm II}$, $S_{\rm III}$, $S_{\rm IV}$, $S_{\rm V}$ are the Seidel coefficients of spherical aberration, coma, astigmatism, field curvature, and distortion, respectively. The other parameters are defined in Fig. 2. For a Czerny-Turner spectrometer, the object is a slit parallel to y-axis. The grating grooves are also parallel to y-axis. Primary aberrations are the main aberrations. The geometrical aberrations of collimating mirror or focusing mirror in parallel beam can be expressed by

$$2\frac{x^2}{f}TA_y = \frac{y(x^2+y^2)}{x^2}S_{\rm I} + \frac{(x^2+3y^2)L+2xyl}{xl}S_{\rm II} + \frac{y(l^2+3L^2)+2xlL}{l^2}S_{\rm III} + \frac{y(l^2+L^2)}{l^2}S_{\rm IV} + \frac{xL(l^2+L^2)}{l^3}S_{\rm V}, \quad (4)$$

$$2\frac{x^2}{f}TA_x = \frac{(x^2+y^2)}{x}S_{\rm I} + \frac{(3x^2+y^2)l+2xyl}{xl}S_{\rm II} + \frac{x(3l^2+L^2)+2ylL}{l^2}S_{\rm III} + \frac{x(l^2+L^2)}{l^2}S_{\rm IV} + \frac{x(l^2+L^2)}{l^3}S_{\rm V}. \quad (5)$$

where f is the focal length of the collimating or condensing mirror, L and l are the horizontal and vertical coordinates of image in the image plane, respectively (see Fig. 2).

For concave spherical mirror, the Seidel aberration coefficients can be easily derived:

$$S_{\rm I} = -\frac{1}{4}\frac{h^4}{f^3}, \quad (6)$$

$$S_{\rm II} = \frac{Jh^2}{2f^2}(1-\frac{z}{2f}), \quad (7)$$

$$S_{\rm III} = -\frac{J^2}{f}(1-\frac{z}{2f})^2, \quad (8)$$

$$S_{\rm IV} = \frac{J^2}{f}, \quad (9)$$

$$S_{\rm V} = -\frac{2Jl^2}{f^3}z(1-\frac{z}{2f})(1-\frac{z}{4f}), \quad (10)$$

where h is the ray height at the surface of the collimating mirror or the condensing mirror, J is the Lagrange invariant, and z is the distance between a concave spherical mirror and a grating.

The geometrical aberrations of Czerny-Turner system are determined by the aberrations of collimating mirror and focusing mirror. So the aberrations of Czerny-Turner system can be expressed by

$$TA_y = TA_{y_1}(\frac{f_2}{f_1})^2 + TA_{y_2}, \quad (11)$$

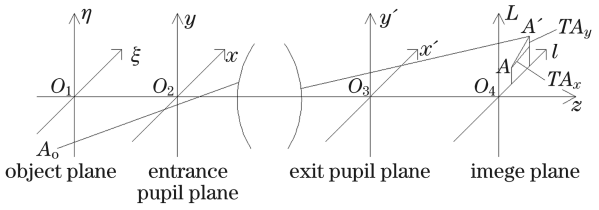

Fig. 2. Coordinate system for calculation of aberrations.

$$TA_x = TA_{x_1}\gamma(\frac{f_2}{f_1})^2 + TA_{x_2}, \quad (12)$$

where f_1 and f_2 are respectively the focal lengths of the collimating and condensing mirrors, TA_{x_1} and TA_{y_1} are the geometrical aberrations of collimating mirror, TA_{y_2} and TA_{x_2} are the geometrical aberrations of focusing mirror, and γ is the angle magnification.

In Czerny-Turner configuration, the centers of grating, image surface, collimating mirror, and focusing mirror are not on the same straight line. So the total geometrical aberrations consist of concentric system aberration TA and nonconcentric system aberration TA_d. Thus the total aberrations are

$$\sum TA_y = TA_y + TA_{dy}, \quad (13)$$

$$\sum TA_x = TA_x + TA_{dx}, \quad (14)$$

where $\sum TA_y$ and $\sum TA_x$ are the total geometrical aberrations.

Any normal of spherical surface can be considered as the optical axis of spherical mirror. So the aberrations in the same focal plane are independent of the choice of optical axis. In Czerny-Turner system, we choose the normals which intersect with the chief rays at mirrors as the optical axes of collimating mirror and focusing mirror. $\bar{x}_1$, $\bar{x}_2$, and $\bar{l}$ are the coordinates independent of the choice of optical axis. Coordinates $\bar{x}_1$ and $\bar{x}_2$ are positioned in incident beam plane and diffracted beam plane perpendicular to grating plane, respectively. The value of coordinate $\bar{l}$ determines the position of spectral line in the image plane, and only depends on the wavelength. When α_1 and α_2 are not too big, we can get the approximate relations:

$$x_1 = \bar{x}_1 + \frac{z}{2}\alpha_1, \quad (15)$$

$$x_2 = \bar{x}_2 + \frac{z}{2}\alpha_2, \quad (16)$$

$$l_1 = -\frac{f}{2}\alpha_1, \quad (17)$$

$$l_2 = \bar{l} + \frac{f}{2}\alpha_2, \quad (18)$$

$$\bar{x}_2 = \frac{\bar{x}_1}{\gamma}, \quad (19)$$

$$y_1 = y_2, \quad (20)$$

$$L_2 = -L_1, \quad (21)$$

where subscripts 1 and 2 denote collimating mirror and focusing mirror, respectively.

Based on Eqs. (4)−(21) we can derive the expressions

for calculating aberrations in the optimum focal plane as follows:

$$2\frac{\bar{x}_2^2}{f}TA_x = \frac{\left[\bar{x}_2^2(\gamma^4+1)+y_2^2(\gamma^2+1)\right]}{\bar{x}_2^2}S_{\rm I} + \frac{\left[(3\bar{x}_2^2+y_2^2)\bar{l}+2y_2\bar{x}_2L(1-\gamma^2)\right]}{\bar{x}\bar{l}}S_{\rm II} + \frac{\left[\bar{x}_2L_2^2(\gamma^2+1)(S_{\rm III}+S_{\rm IV})\right]}{\bar{l}^2} + \frac{2y_2L_2}{\bar{l}}S_{\rm III}, \quad (22)$$

$$2\frac{\bar{x}_2^2}{f}TA_y = \frac{y_2\left[\bar{x}_2^2(\gamma^2+1)+2y_2^2\right]}{\bar{x}_2^2}S_{\rm I} + \frac{\left[2y_2\bar{l}+\bar{x}_2L_2(1-\gamma^{2)})\right]}{\bar{l}}S_{\rm II} + \frac{\left[2y_2L_2^2(S_{\rm III}+S_{\rm IV})\right]}{\bar{l}^2} + \frac{2(\bar{x}_2L_2-y_2\bar{l})}{\bar{l}}S_{\rm III}, \quad (23)$$

$$2fTA_{dx} = -\frac{1}{4}[3\bar{x}_2^2(\gamma^3\alpha_1-\alpha_2)+y_2^2(\gamma\alpha_1-\alpha_2)] - y_2L_2(\gamma\alpha_1+\alpha_2)(1-\frac{z}{2f}), \quad (24)$$

$$2fTA_{dy} = -\frac{1}{2}\bar{x}_2y_2(\gamma\alpha_1-\alpha_2) - [\bar{x}_2L_2(\gamma\alpha_1+\alpha_2)-2y_2\bar{l}\alpha_2]\times(1-\frac{z}{2f}) + yf(\gamma^2\alpha_1^2+\alpha_2^2). \quad (25)$$

In Eqs. (24) and (25), the first terms represent the nonconcentric second-order coma, the second terms represent the nonconcentric second-order astigmatism. In Eq. (25), the third term represents the nonconcentric first-order astigmatism. The height of entrance slit is less than the size of grating and image plane, so we can replace L_2^2 with 0. Moreover, In Eqs. (7) and (8), if z=2f, $S_{\rm II}$= $S_{\rm III}$=0. So we can obtain the approximate aberration expressions:

$$2\frac{\bar{x}_2^2}{f}TA_x = \frac{\left[\bar{x}_2^2(\gamma^4+1)+y_2^2(\gamma^2+1)\right]}{\bar{x}_2^2}S_{\rm I}, \quad (26)$$

$$2\frac{\bar{x}_2^2}{f}TA_y = \frac{y_2\left[\bar{x}_2^2(\gamma^2+1)+2y_2^2\right]}{\bar{x}_2^2}S_{\rm I}, \quad (27)$$

$$2fTA_{dx} = -\frac{1}{4}[3\bar{x}_2^2(\gamma^3\alpha_1-\alpha_2)+y_2^2(\gamma\alpha_1-\alpha_2)], \quad (28)$$

$$2fTA_{dy} = -\frac{1}{2}\bar{x}_2y_2(\gamma\alpha_1-\alpha_2)+y_2f(\gamma^2\alpha_1^2+\alpha_2^2). \quad (29)$$

As we can see in Eqs. (26)−(29) the aberrations are independent of $\bar{l}$, namely independent of wavelength. Thus, using the geometrical aberration theory we find that the grating should be coplanar with the centers of curvature of both mirrors. The condition guarantees that the aberrations are independent of wavelength. Moreover, the condition does not depend on image surface size, groove density of the grating, and focal length of the mirrors. Therefore, the aberrations are constant over a broad spectral range.

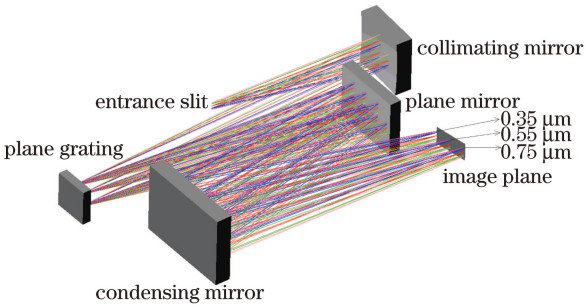

Fig. 3. Layout of the Czerny-Turner imaging spectrometer system.

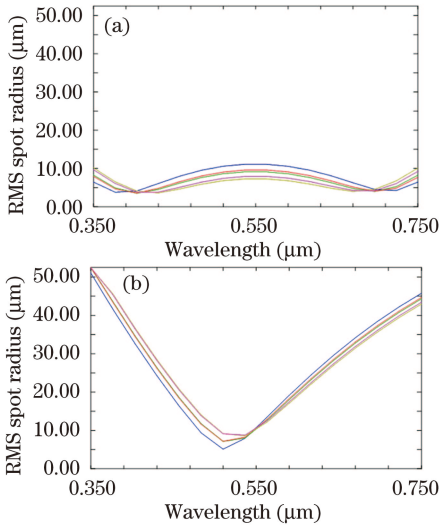

Fig. 4. RMS spot radius versus wavelength for (a) the modified and (b) the existing Czerny-Turner configurations. Different curves stand for the results obtained with different fields of view.

In the following, we give an example to illustrate the application of the modified arrangement. It is a Czerny-Turner imaging spectrometer with a fixed plane grating (300 l/mm) and the following specifications: effective focal length 69 mm, $F/8$, and slit size 50 μm ×5 mm. The spectrometer is an ultraviolet (UV) to visible system with a broadband spectral range from 0.35 to 0.75 μm. A CCD with a size of 25 × 25 (mm) is employed. The design wavelength is the center wavelength (0.55 μm). To diminish the geometrical scale of the spectrometer, we place a plane mirror between the grating and a focusing mirror. The optical structure of the system is shown in Fig. 3. The optical system design program ZEMAX is used to model and analyze the system.

With the help of the program ZEMAX, the optical performance of the system can be predicted and plotted. Spot diagrams at the detector surface are calculated for different fields of view at the entrance slit with our modified and the existing Czerny-Turner configurations. To show that the best position of the grating is critically important for obtaining excellent aberration properties over a broadband spectral range, we compare the

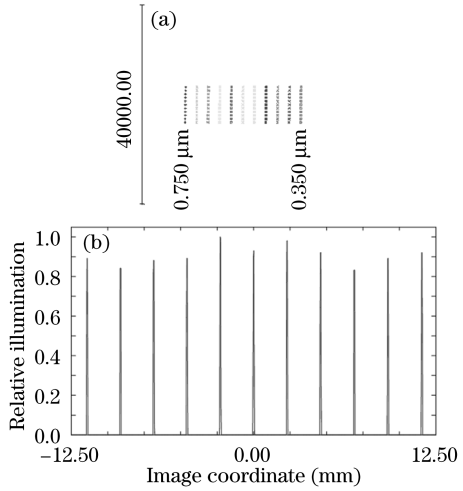

Fig. 5. Simulation results of imaging spectra. (a) Imaging surface's full field spot diagram; (b) irradiance map for all the sample wavelengths on CCD's light sensor surface.

Table 1. Optical Parameters of the Imaging Spectrometer

Specification	Optimized by Ray Tracing (at 0.55 μm)
r_1 (mm)	240
r_2 (mm)	360
$\alpha_1/2$ (deg.)	5
$\alpha_2/2$ (deg.)	10
i (deg.)	−1
θ (deg.)	10.513
$L_{\mathrm{es-cl}}$ (mm)	119.543
$L_{\mathrm{cl-g}}$ (mm)	239.087
$L_{\mathrm{g-fc}}$ (mm)	354.531
$L_{\mathrm{fc-im}}$ (mm)	177.8

r_1 and r_2 are the radii of curvature of the collimating and condensing mirrors. $L_{\mathrm{es-cl}}$, $L_{\mathrm{cl-g}}$, $L_{\mathrm{g-fc}}$, and $L_{\mathrm{fc-im}}$ are the distances between the entrance slit and the collimating mirror, the collimating mirror and the grating, the grating and the focusing mirror, and the focusing mirror and the image plane, respectively.

aberration properties in our modified arrangement with that in the existing arrangement. The root-mean-square (RMS) spot radius is given as a function of wavelength. Obviously, when the grating is coplanar with the centers of curvature of collimating mirror and focusing mirror (namely, $L_{\mathrm{cl-g}}$=$2f_{\mathrm{T1}}$, $L_{\mathrm{g-fc}}$=$2f_{\mathrm{T2}}$, $L_{\mathrm{cl-g}}$ and $L_{\mathrm{g-fc}}$ are the distances from the collimating mirror to the grating and from the grating to the focusing mirror, f_{T1} and f_{T2} are the tangential focal lengths of the collimating and condensing mirrors, respectively), good imaging quality is obtained over the entire spectral range, as shown in Fig. 4(a). However, in existing arrangement ($L_{\mathrm{cl-g}} \approx f_{\mathrm{T1}}$, $L_{\mathrm{g-fc}} \approx f_{\mathrm{T2}}$), good imaging quality is obtained only in the vicinity of the center wavelength, as shown in Fig. 4(b).

The optical parameters of the imaging spectrometer is shown in Table 1. Setting the sample wavelengths between 0.35 and 0.75 μm with an interval of 40 nm, the simulation results of imaging spectra are shown in Figs. 5(a) and (b). Figure 5(a) is the imaging surface's full field spot diagram, Fig. 5(b) is the irradiance map for all the sample wavelengths on CCD's light sensor surface. Figure 5(a) shows that this design's imaging spots are of good quality; the imaging spectrum also has good linearity which demonstrates that the system's coma and astigmatism are well eliminated. Figure 5(b) shows that imaging spots' power of each wavelength are nearly the same throughout the working wavelength range when neglecting CCD's efficiency. This means that the system's optical structure has remarkable imaging quality, thereby ensures a high spectral resolution.

In conclusion, a novel variety of Czerny-Turner spectrometer is proposed to obtain broadband spectral simultaneity by analyzing the dependence of aberrations for different wavelengths. A practical example is given, and the excellent performance of the imaging spectrometer is confirmed by simulation in ZEMAX software. The arrangement is larger than the existing configuration, but it is recommended for imaging spectrometer with a short focal length and a broadband spectral region.

This work was supported by the National Natural Science Foundation of China under Grant No. 40675083.

References

1. A. B. Shafer, L. R. Megill, and L. Droppleman, J. Opt. Soc. Am. **54,** 879 (1964).
2. J. Wang, S. Wang, and G. Lin, Chin. Opt. Lett. **6,** 510 (2008).
3. F. Si, P. Xie, C. Liu, J. Liu, Y. Zhang, K. Dou, and W. Liu, Chin. Opt. Lett. **6,** 541 (2008).
4. L. Zhou, Y. Wu, P. Zhang, M. Xuan, Z. Li, and H. Jia, Opt. Prec. Eng. (in Chinese) **14,** 990 (2006).
5. L. Zhou, Y. Wu, P. Zhang, M. Xuan, H. Jia, and Z. Li, Opt. Prec. Eng. (in Chinese) **13,** 637 (2005).
6. R. R. Conway, M. H. Stevens, C. M. Brown, J. G. Cardon, S. E. Zasadil, and G. H. Mount, J. Geophys. Res. **104,** 16372 (1999).
7. R. D. McPeters, S. J. Janz, E. Hilsenrath, T. L. Brown, D. E. Flittner, and D. F. Heath, Geophys. Res. Lett. **27,** 2597 (2000).
8. M. R. Torr and D. G. Torr, Appl. Opt. **34,** 7888 (1995).
9. M. G. Dittman, J. Leitch, M. Chrisp, J. V. Rodriguez, A. Sparks, B. McComas, N. Zaun, D. Frazier, T. Dixon, R. Philbrick, and D. Wasinger, Proc. SPIE **4814,** 120 (2002).
10. Z. Wang, *Theory Fundamentals of Optical Design* (2nd edn.) (in Chinese) (Science Press, Beijing, 1985).